Available online at www.sciencedirect.com
ScienceDirect
Journal of Catalysis 249 (2007) 41–51
JOURNAL OF CATALYSIS
www.elsevier.com/locate/jcat

Imaging promoter atoms in Fischer–Tropsch cobalt catalysts by aberration-corrected scanning transmission electron microscopy

Mervyn D. Shannon [a,b,*], C. Martin Lok [c], John L. Casci [c]

[a] *ICI Measurement Science Group, Wilton Center, Redcar, Cleveland, TS10 4RF, UK*
[b] *UK SuperSTEM Facility, CLRC Daresbury Laboratories, Keckwick Lane, Warrington, WA4 4AD, UK*
[c] *Johnson Matthey Catalysts, PO Box 1, Billingham, Cleveland, TS23 1LB, UK*

Received 27 September 2006; revised 28 February 2007; accepted 22 March 2007

Available online 21 May 2007

Abstract

The location and distribution of the promoters in reduced and passivated cobalt catalysts were investigated using the "SuperSTEM" aberration-corrected scanning transmission electron microscope, which passes the 1-Å resolution threshold. Atomic number contrast imaging was achieved using a high-angle annular dark-field detector and elemental spectroscopy, with close to 0.1 nm spatial resolution, using electron energy-loss spectroscopy. The catalyst investigated was the newly developed 20% Co-on-alumina Fischer–Tropsch catalyst prepared via the cobalt ammine carbonate deposition-precipitation route. The catalyst was postimpregnated, after drying, with Pt, Ir, Re, or Ru promoter precursors. Whereas only Ru, Pt, and Ir were effective in lowering the temperature for the conversion of Co_3O_4 to CoO, all four elements promoted the further reduction to metallic cobalt. All of the promoters applied increased the Co surface area, the greatest improvement being with Ir. The microscopy results show the Re, Pt, and Ir promoters mainly as isolated atoms, whereas Ru was present in regions of high concentration within Co particles. Because even promoter-free cobalt particles (within the promoted samples) seem to undergo reduction promotion, the results are consistent with hydrogen spillover as a mechanism for reduction promotion.

Keywords: Cobalt; Alumina; Fischer–Tropsch; Promoters; Aberration-corrected; Atomic resolution; STEM; EELS

1. Introduction

Individual atoms were first imaged by scanning transmission electron microscopy (STEM) by Crewe in 1973 [1]. The atoms detected were uranium on a very light amorphous substrate of carbon. The contrast in the high-angle angular dark field image (HAADF) was high because of the approximate Z^2 dependence of the scattering power with atomic number Z. The focused electron probe was of the order of 0.3 nm diameter, and thus the definition of the uranium atom positions was not very precise.

The advent of aberration-corrected STEM in the last few years has made it possible to form imaging probes of 0.1 nm diameter or better [2]. This not only allows better location of atom positions, but also enables experiments in which the atomic number difference is much smaller. This relates to the higher current density at the scattering atom, which gives further improved contrast and signal-to-noise ratio.

With this development, it is timely to consider whether or not heavy promoter atoms in catalyst formulations can be imaged and their role further elucidated. For example, platinum group metals (PGMs) are commonly used to promote Co-based Fischer–Tropsch (FT) catalysts. Depending on the PGM chosen, this can either act to lower the temperature of reduction of the oxide (and thus preserve high surface area) or to alter the surface configuration [3]. The motivation for this study was to determine whether questions such as (1) where on the surface do the promoter atoms sit, (2) are any of them buried within cobalt particles during reduction, (3) do they form clusters of promoter atoms, and (4) are they confined to the cobalt phase or present on the support, can be addressed by direct imaging.

As gas to liquid technology, including FT catalysis, is predicted to grow to a multi-billion dollar global business, the need to understand promotion to more effectively use cobalt

* Corresponding author. Fax: +7843 295885.
E-mail address: mervyn_shannon@ici.com (M.D. Shannon).

0021-9517/$ – see front matter
doi:10.1016/j.jcat.2007.03.021

and the rare and expensive PGMs is paramount (see [4] for example). Iglesia [5] concluded that Fischer–Tropsch turnover rates were independent of Co dispersion in a certain dispersion range (0.01–0.12) at typical Fischer–Tropsch conditions, and thus cobalt surface areas should be indicative of activity. Lok [6] also reported that the activity of Co catalysts was proportional to metal surface area up to high loadings and with high dispersion. However, recent work by the De Jong group in Utrecht concluded that the Fischer–Tropsch reaction was structure-sensitive for high cobalt dispersions. They stated that both selectivity and activity changed for carbon nanofiber-supported catalysts with particles smaller than 6 nm [7]. The Co particles in this study are in this size range.

There is a considerable literature on the physical characterisation of Co catalysts. Of particular relevance is the work of Davis and co-workers [8] on EXAFS/XANES studies of the effect of Re promotion on the reduction of Co/Al_2O_3 catalysts. These authors found direct contact between Re and Co atoms but no evidence of Re–Re bonds or Re–support interactions. More recently, these same authors reported similar results on Pt promotion [9].

Some work has already been reported on the imaging of isolated dopant atoms in other systems by aberration-corrected STEM [10–12]. But these were somewhat ideal samples of antimony-doped silicon, lanthanum-doped alumina, and lanthanum-doped calcium titanate. The matrices in these experiments have a much lower atomic number than cobalt metal. Moreover, the samples were either uniformly thick or a controlled wedge, whereas the catalysts samples reported here are aggregated particles, with each particle a few nm in size. In one study [12], the identity of the heavy dopant atom was confirmed by electron energy-loss spectroscopy (EELS).

In earlier work, we outlined our initial findings on aberration-corrected STEM imaging of PGM-promoted Co Fischer–Tropsch catalysts [13]. Bezemer et al. [14,15] have studied manganese-promoted FT catalysts in such an instrument but without resolving individual atoms. Li et al. [16] reported an EELS and EDX study by conventional (i.e., not aberration-corrected) FEG-(S)TEM of a 3 wt% Ru-promoted catalyst (20 wt% Co on γ-alumina). The sample was reduced in situ under 20 Pa of pure H_2 at 400 °C for 3 h. After the in situ reduction, they found a bimodal distribution of particle sizes centered at about 1 and 7 nm and noted that the smaller Co particles contained a much greater proportion of Ru. They also observed that the larger particles arose by sintering of the smaller ones. More recently [17], these authors reported a further in situ TEM/STEM study of the direct reduction in 10% H_2/90% N_2 at 400 °C for 3 h of 20% Co and 20% Co, 2% Ru samples supported on γ-alumina from cobalt nitrate hexa-hydrate and, in the latter, co-precipitated ruthenium chloride. In the promoted sample, only particles containing Ru where observed to reduce to metal.

2. Experimental

Samples were made based on a 20 wt% Co-on-alumina catalyst prepared by deposition–precipitation at high pH using a cobalt ammine complex (high-dispersion cobalt [HDC] method [6,18,19]). The support was γ-alumina Puralox HP14/150, obtained from Sasol unless indicated otherwise. In some cases, θ-alumina prepared by calcination of the γ-alumina at 1050 °C was used. The dried catalyst was split into four parts, and each part was postimpregnated with one of the most commonly reported PGM promoters (Ru, Re, Ir, or Pt) before drying, calcination at 280 °C (Re, Ir, Pt) or 350 °C (Ru), and finally reduction at 425 °C for 6 h. The four samples contained 1 wt% Ru from Ru(III) nitrosylnitrate in water, 1 wt% Re from perrhenic acid in water, 0.3 wt% Ir from Ir(III) acac in acetone, and 0.3 wt% Pt from Pt(II) acac in acetone.

Temperature-programmed reduction (TPR) was carried out in a reduction gas stream comprising 5% hydrogen in nitrogen. The sample (0.1–0.15 g, accurately weighed) was first heated to 120 °C (at 5 °C/min under a reduction gas flow of 25 mL/min) to remove moisture and held at 120 °C for 45 min. Thereafter, the sample was heated from 120 to 1000 °C in the reduction gas stream at a heating rate of 5 °C/min. The change in concentration of hydrogen between the inlet gas and the outlet gas was monitored by a katharometer to show the consumption of hydrogen at each temperature. A Quantachrome ChemBet TPR/TPD analyzer was used for the TPR measurements.

The cobalt surface area was determined by H_2 chemisorption according to the following procedure. Approximately 0.2–0.5 g of sample material was first degassed and dried by heating to 140 °C at 10 °C/min in flowing helium and maintaining at 140 °C for 60 min. The degassed and dried sample was then reduced by heating it from 140 to 425 °C at a rate of 3 °C/min under a 50 mL/min flow of hydrogen and then maintaining the hydrogen flow at 425 °C for 6 h. After this reduction, the sample was heated under vacuum to 450 °C at 10 °C/min and held under these conditions for 2 h. The sample was then cooled to 150 °C and maintained for a further 30 min under vacuum. The chemisorption analysis was then carried out at 150 °C using pure hydrogen gas. An automatic analysis program was used to measure a full isotherm at 1.3–100 kPa hydrogen pressure. The analysis was carried out twice. In the first analysis, the "total" hydrogen uptake (including chemisorbed hydrogen and physisorbed hydrogen) was measured. Then the sample was immediately put under vacuum (<5 mm Hg) for 30 min, and the analysis was repeated to measure the physisorbed uptake. A linear regression was then applied to the "total" uptake data with extrapolation back to zero pressure to calculate the volume of gas chemisorbed (V).

Cobalt surface areas were calculated in all cases using the following equation [20]:

$$\text{Co surface area} = \frac{6.023 \times 1023 \times V \times \text{SF} \times A}{22414},$$

where V represents uptake of H_2 (in mL/g), SF is the stoichiometry factor (assumed to be 2 for H_2 chemisorption on Co), and A is the area occupied by one atom of cobalt (assumed to be 0.0662 nm^2).

XRD analysis was performed on a Siemens D5000 theta–theta X-ray diffractometer equipped with a Baltic Scientific Instruments Sol-X energy-dispersive detector. Copper $K\alpha$ radiation was used. The XRD specimens were prepared under

nitrogen in standard bulk front fill holders. The X-ray beam divergence was controlled by a programmable slit to give 12-mm-long illumination of the specimen surface. A 0.6-mm receiving slit was used together with primary soller slits. The data were collected for an angular range of 2–75° 2θ. A rapid scan was done for initial measurements with and without a PET dome, with a step size of 0.1° 2θ and a count time of 1 s per step, followed by a slower scan with a step size of 0.05° 2θ and a count time of 1.2 s per step. During the reduction experiments, a flow of 4% H_2 in N_2 was passed through the sample in an Anton Paar reaction chamber at a rate of ca. 30 mL/min.

All of the reductions were performed at atmospheric pressure. The degree of reduction was much higher than that reported for in situ TEM studies [16,17].

For microscopy after the reduction procedure in the chemisorption apparatus, the surface of each sample was passivated using 1% O_2 in N_2 at 35 °C for 16 h, discharged under nitrogen into suitable sealed containers and then transported in a few hours or overnight to the UK SuperSTEM facility. Each sample was lightly ground in air, dusted onto a lacy carbon support film, and transferred to the microscope with a dwell time at atmospheric pressure of about 5 min. Generally it was left overnight in the imaging position to stabilize specimen drift.

The UK SuperSTEM facility houses a VG HB501 enhanced by the addition of a Nion third-order aberration corrector [21] that largely compensates for spherical aberration—the major inherent aberration of round lenses that has hitherto limited the resolution of electron microscopes. The instrument routinely achieves 0.1 nm resolution or better.

HAADF and bright field (BF) detectors were used to form images. The former captures electrons scattered between 70 and 210 mrad and at 100 keV is of sufficiently high angle to exclude elastically diffracted beams and essentially detect thermal diffuse scatter. As a consequence, HAADF images are dominated by scatter that is approximately proportional to Z^2 and so are most sensitive to elements of high atomic number. Indeed, light atoms can be very hard to detect in this signal. The BF image is much more sensitive to the light elements, and the two images recorded simultaneously are truly complementary. The BF image is also very useful for preliminary focusing because it is stronger and has a higher S/N ratio.

The HAADF signal is also proportional to sample thickness. So, to more easily distinguish isolated heavy atoms from thickness variation associated with particle shape, differentiation in the x-direction was applied. This was achieved by using a combination of smoothing operator and a Kirsch 3 × 3 east–west convolution filter on the HAADF images. These atoms have a white–black contrast from left to right. An atomic column with a heavy promoter atom will give greater white–black contrast in these than one without. It also has the merit of removing much of the streaking and noise in the HAADF image due to inherent fluctuations in electron emission from the microscope's cold-field emitter.

A Gatan Enfina EELS provided elemental analysis using the same 0.1-nm probe as for imaging. Energy-dispersive X-ray microanalysis (EDX) was not fitted to the instrument. The electron current in the probe was adjusted using the extraction voltage,

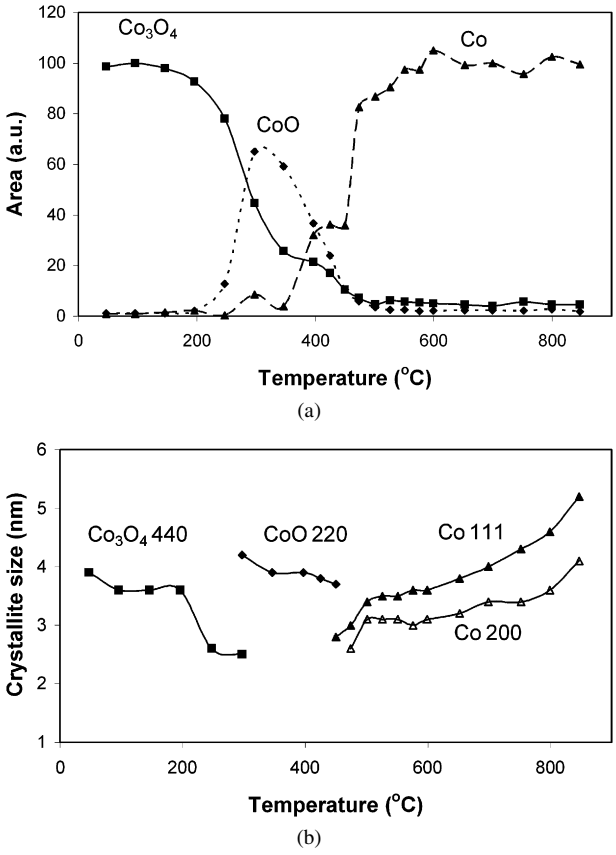

Fig. 1. In situ XRD reduction by 4% H_2 in N_2 showing (a) the percentage of each phase, Co_3O_4, CoO and Co metal, present as a function of temperature and (b) the crystallite size derived from analysis of the peak shapes.

and the electron dose was controlled by pixel density and dwell time. The spectra were recorded using spectrum imaging, in which a full spectrum is gathered at each pixel in a scanned subarea of an image and stored as a data cube for processing to provide element maps.

Of the PGM metals studied here, only Ru can be readily analyzed by EELS. The most definitive absorption edge for analysis of Re, Ir, and Pt—$M_{4,5}$—is around 2000 eV and thus of very low intensity. Because the samples are not stable under a high current flux, we have attempted to use the much lower-energy $N_{6,7}/O_{2,3}$ edges in the range of 40–50 eV. This is complicated by the presence of the Co $M_{2,3}$ edge at 60 eV and, more problematically, by collective oscillations such as bulk and surface plasmon excitations.

3. Results

In situ X-ray diffraction (Fig. 1) demonstrated that reduction in 4% H_2/N_2 at atmospheric pressure took place in two stages, with Co_3O_4 reduction to CoO initiating by 250 °C and CoO to Co initiating by 400 °C and reaching completion around 600 °C [22]. Careful line-broadening studies indicated that the HDC route converted each Co_3O_4 crystal to a CoO crystal and then to a Co metal particle without sintering. This study showed that below 600 °C, the Co particle size remained <4 nm. A separate HRTEM study of a related unpromoted reduced sample

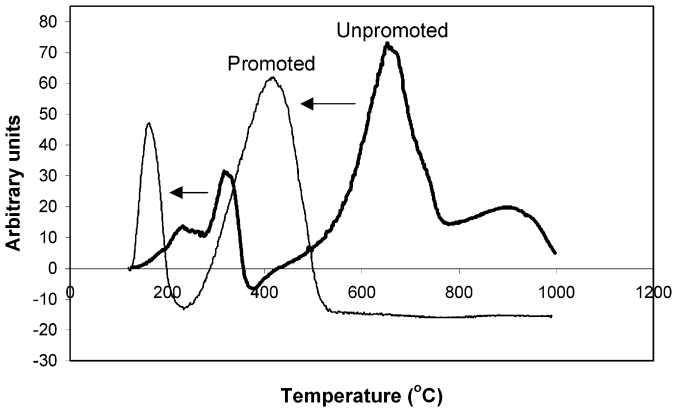

Fig. 2. An example of the effect of a promoter on the reduction. The darker line is for unpromoted catalyst and the lighter line is for Ru promoted catalyst.

Table 1
Temperature maxima for promoted and unpromoted 20% Co-on-alumina catalyst in temperature programmed reduction

Promoter	Co(III) to Co(II) (°C)	Co(II) to Co(0) (°C)
None	320	660
1.0% Re	330	545
1.0% Ru	168	420
0.3% Pt	245	474
0.3% Ir	256	470

Table 2
Cobalt surface area measurements for series of experiments where 20% cobalt precursor oxide on alumina samples were split, promoted and investigated as indicated in the table. A and B refer to two different batches of the same HP 14/150 γ-alumina

Base catalyst	Promoter	Co SA [tot0] (m^2/g_{cat})
20% Co on γ-alumina batch A	None	16.4
	Ru—1%	18.7
	Ir—0.3%	20.2
	Pt—0.3%	18.0
20% Co on γ-alumina batch B	None	17.6
	Re—1%	19.3
20% Co on θ-alumina (θ-alumina derived from batch B)	None	19.1
	Ru—1%	22.6
	Ir—0.3%	24.2

based on theta alumina showed Co particle sizes in the range of 2–6 nm (mean size ca. 3.8 nm). TPR measurements indicated that Ru, Ir, and Pt, but not Re, lowered the temperature of the Co(III)-to-Co(II) transition, and all lowered the temperature for reduction of Co(II) to Co(0) (Table 1; Fig. 2). The promoters applied in this manner also affected the Co surface area (Table 2), generating increases of 10% or more in all cases.

An example of the distribution of heavy atoms in a calcined Re-promoted catalyst is shown in Fig. 3. Many bright features of the size of a single atom are seen and can be taken to be rhenium. There are also suggestions of small clusters of Re atoms, although there is clearly some sample charging and drift, which may cause some single atoms to be imaged as a small patch in the rastered image. The HAADF intensity profile Fig. 3c is one example that more clearly indicates the contast obtained from the heavy atom. It is taken along the line indicated in Fig. 3a from the outer ends of the lines.

In the corresponding reduced and passivated sample, however, the heavy atoms are less readily detected (Figs. 3d–3f) but are most commonly isolated atoms. We discuss the reasons for this in detail below. For now, we point out that the mean atomic number of cobalt oxide (Co_3O_4) is about 16, compared with 27 for cobalt metal. Therefore, the expected contrast between isolated rhenium atoms and the average atom in the cobalt phase changes by roughly a factor of 3–4 from oxide to metal, and thus a drop in visibility might be expected.

Most of the images obtained showed dopant atoms either without a resolved crystal lattice or on the ridge of 1-dimensional lattice fringes, but not at a zone–axis orientation. The higher magnification image shown in Fig. 3g was obtained on the [110] zone axis of a cobalt particle showing two Co columns with enhanced intensity, each of which, we contend, contains a Re. Furthermore, these atoms occupy Co lattice sites.

For the passivated samples, similar results as for Re were obtained for both Pt and Ir (Fig. 4). Based on the given promoter and metal loadings, Co particles of 3 nm diameter would contain approximately 20–25 Re promoter atoms or 7–8 Pt or Ir atoms, whereas those of 4 nm diameter would contain more than double these amounts. (Obviously, we did not image all of the promoter atoms.) To obtain useful information on the mechanism of promotion, we need to understand why this occurs and either take this into account when interpreting the data or find a new way to reveal the location of all of the promoter atoms.

The positions of the bright atom-sized features tend to change in repeated scans, suggesting that these heavy atoms are on or in the surface of the particles. These features were generally not observed to be weighted toward the edge (of the projection image) of the Co particles, as would be expected for a surface distribution; however, an example of this feature is shown around the 2-nm particle near the center of Figs. 4a and 4b.

The bright atom-sized features that are seen occur at Co lattice sites, not interstitial sites. The contrast between a single interstitial PGM atom and a column of Co atoms will favor Co in particles larger than 1 nm, as is the case here. This general point was made by Voyles et al. [10] in relation to thin antimony-doped silicon foils. Only near the thin edge of the Co particles (as seen in projection on STEM) can interstitial atoms be imaged with high contrast. Again, in this study, bright atom-sized features at the edge of Co particles were rare. Complementary BF imaging is important to detect any interstitial atoms.

The catalyst supports are γ- or θ-alumina, which are insulating. Thus, each sample was prone to charging and hence image drift. There is also a tendency toward damaging the alumina under the electron beam. Therefore, an analysis method to identify the atom(s) giving rise to bright features must involve only a low dose. The $M_{4,5}$ edges for Re, Ir, and Pt at ca. 2000 eV are so low in intensity that a much higher electron dose is required for detection than the sample can tolerate without extensive drift and/or damage. Consequently, the low loss region, 30–90 eV,

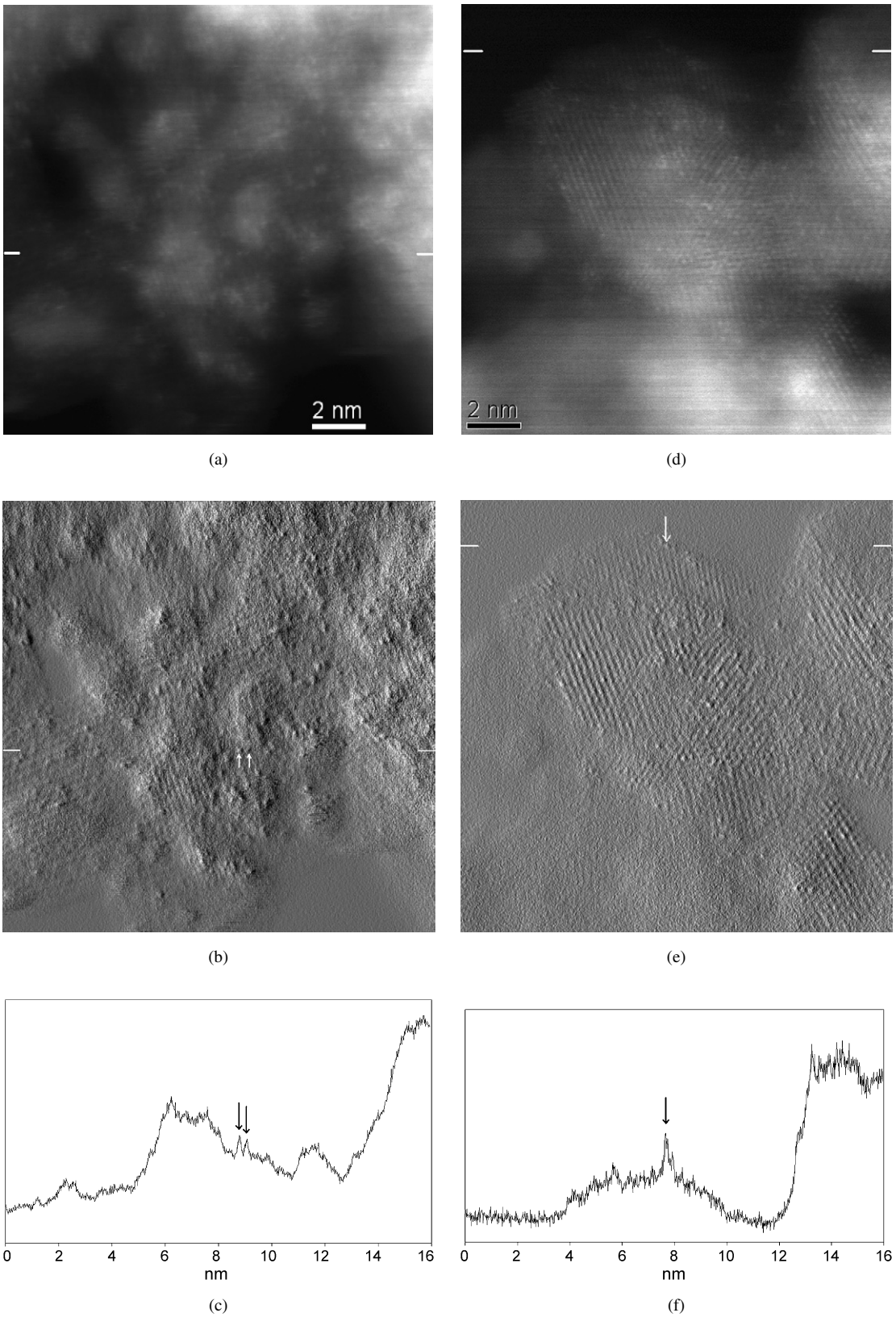

Fig. 3. Examples of HAADF images of 1% Re promoted catalyst calcined in (a), (b), and (c) and reduced and passivated in (d), (e), (f), and (g). Images (b) and (e) are derived from (a) and (d) by smoothing and application of a Kirsch East filter. Intensity profiles (c) and (f) are extracted along the indicated lines in (a) and (d), respectively, with dopant atom positions arrowed. In (g) dopant atoms (arrowed) are observed in a Co [110] zone-axis orientation are shown; the line profile being averaged between the white lines on the image. The ticks on the abscissa are 1 nm apart.

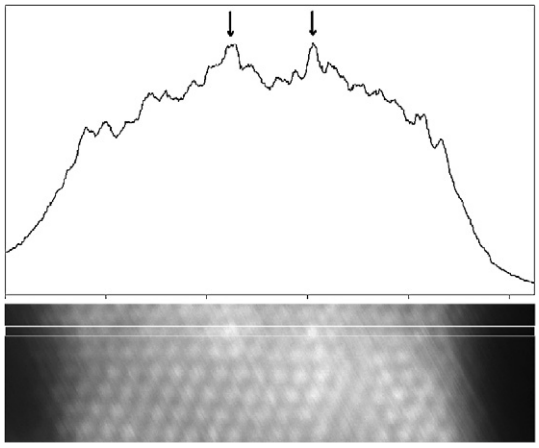

(g)

Fig. 3. (*continued*)

has been explored for all of the promoters (Fig. 5). The range includes the $O_{2,3}$ edge for Re, Ir, and Pt and the $N_{2,3}$ edge for Ru. Ruthenium has a significantly lower atomic number than the others and also has a useful M edge beginning at 275 eV and rising slowly but with an increasing rate to give a maximum gradient at around 300 eV (Fig. 6). This is much more intense than the M edges for the other higher-atomic number promoters.

For ruthenium, we observed occasional bright atom-sized features in the HAADF signal (Fig. 7) and "patches" of Ru by EELS spectrum imaging (Fig. 8). The Ru clusters are generally associated with a cobalt particle; however, the Ru loading is much higher than that of the other promoters in terms of numbers of atoms. Some Co particles, such as the one to the right in Fig. 8a, do not contain a Ru cluster.

The measured Ru in the largest Co particle in Fig. 8a corresponds to 1 in 10 atoms overall being Ru and at most to 2 Ru atoms in or on a column of Co, possibly one top and one bottom. Based on this finding, we have sufficient sensitivity to detect a single isolated Ru atom in the smaller particle to the right. Provided that isolated Ru atoms do not move under the influence of the electron beam, this particle indeed would appear to be promoter-free. The largest particle is clearly a metal; the O-K edge signal falls to zero at the center of the particle. There is no sharp peak at threshold of the O-K edge in the other spectra from this particle or in those from the Ru-free particle (Fig. 8a). Li et al. [17] stated that the presence of such a peak would indicate oxidized Co rather than O from the alumina support. They suggested that Co_3O_4 and CoO both gave rise to this sharp feature at the edge; however, the results of Wang et al. [23] showed that the feature is very weak in CoO. Thus, the evidence indicating that the Ru-free Co particles here are Co metal rather than unreduced CoO is that the O-K signal does not rise as the probe crosses from alumina support to support plus Co-containing particles. Indeed, for the Ru-free particle in Fig. 8a, it falls, and the O:Co atomic ratio is much lower than 1 at the center of this particle.

Using spectrum imaging in the low energy-loss region detected apparent isolated Ru particles on the alumina support [13]. However, the Ru-$N_{2,3}$ edge is so intense that the Co signal that sits on top of it (Fig. 5) is extremely difficult to extract. Indeed, that spectrum corresponds to a relatively low Ru content. Furthermore, the EELS cross-sections in this energy range are not available for the shell (Ru-N) or experimental geometry (Co-M). At present, the best that can be said is that there were very small ($\ll$2 nm) Co particles associated with $>$30 at% Ru on the alumina support in this sample. This estimate is based on inaccurate extraction of the Co-M signal, its inaccurate cross-section, and the Ru-M signal recorded simultaneously.

Without definitive EEL spectra from the isolated atoms detected in the HAADF images of this sample, we cannot be 100% certain that these are Ru and not an occasional heavy impurity atom. These show surprisingly strong contrast for a single Ru atom, as strong as that from the heavier PGM atoms. No spectrum image subsequently acquired from an area displaying bright atoms indicated an association with the substrate alumina rather than cobalt. This last statement is also true for the heavier promoters Re, Ir, and Pt. Because the contrast between promoter and alumina would be expected to be much greater than between promoter and cobalt, this is a highly significant result. Isolated atoms are not observed on the alumina support in any of the reduced and passivated samples. Clusters of atoms are observed only in the case of ruthenium and are associated with Co on the alumina support.

Limited EELS characterization of the calcined Re-promoted sample was undertaken to distinguish Co_3O_4 from γ-alumina at low magnification. No definitive evidence was found at high magnification to establish the phase with which the heavy atoms (Fig. 3a) are associated.

4. Discussion

4.1. HAADF imaging

Consider the following highly simplified model. Let the scattering into the HAADF detector be proportional to Z^2 for the promoter and to z^2 for the "average atom" within the particle that the promoter atom is on or in. The average atom is Co in cobalt metal ($z = 27$) and 3/7 Co plus 4/7 O in the oxide ($z = 16$). Furthermore, suppose that there are n of these average atoms in the column containing the promoter atom and n average atoms but no promoter atoms in a neighboring column. If the scattering of each atom is additive, then the former has scattered intensity proportional to $Z^2 + nz^2$ and the latter intensity proportional to nz^2. So the contrast, C, between the columns (ratio of intensities) would be given by

$$C = \frac{Z^2 + nz^2}{nz^2} = 1 + \frac{1}{n} \cdot \frac{Z^2}{z^2}.$$

For a small particle (3 nm diameter) and atom separations along the column of, say 0.2 nm, this would imply that $C \sim 1.5$ for Re and Co and $C \sim 2.5$ for Re and Co_3O_4. Thus, for metal or oxide particles of this size, the contrast should easily be sufficient to detect the promoter atoms. But we do not measure such strong contrast. On this model, the scattering intensity for n atoms of Co in a column is proportional to nz^2. This proportionality to

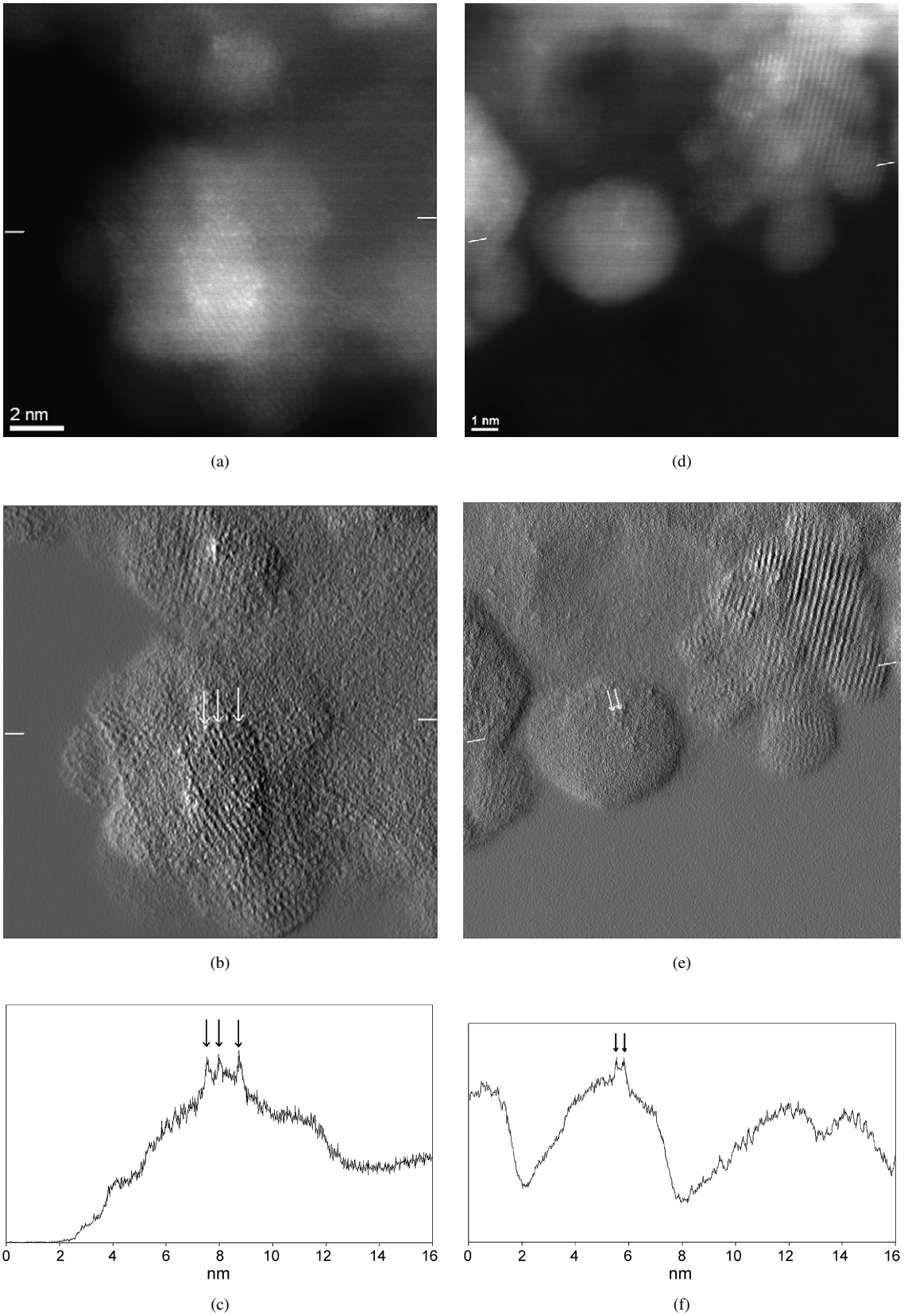

Fig. 4. Examples of HAADF images of reduced and passivated samples of 0.3% Pt-promoted 20% Co on γ-alumina (a–c) and 0.3% Ir-promoted 20% Co on θ-alumina catalyst (d–f). See Fig. 3 caption for details.

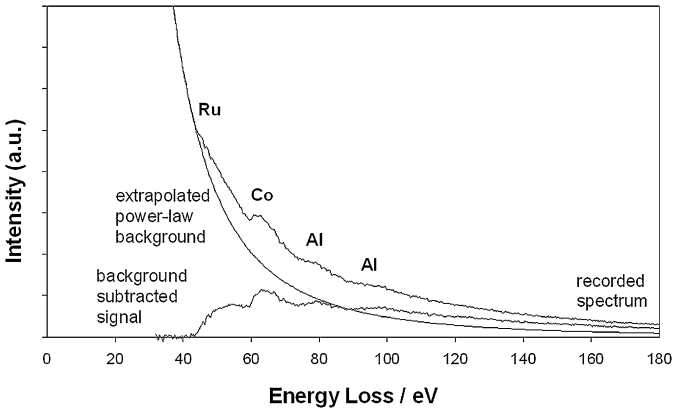

Fig. 5. Low loss region of an EEL spectrum for an Ru containing particle showing the recorded spectrum, the power law background fitted to the pre-edge and the spectrum minus this background. Re, Ir and Pt have $N_{6,7}/O_{2,3}$ edges in the range 40–50 eV.

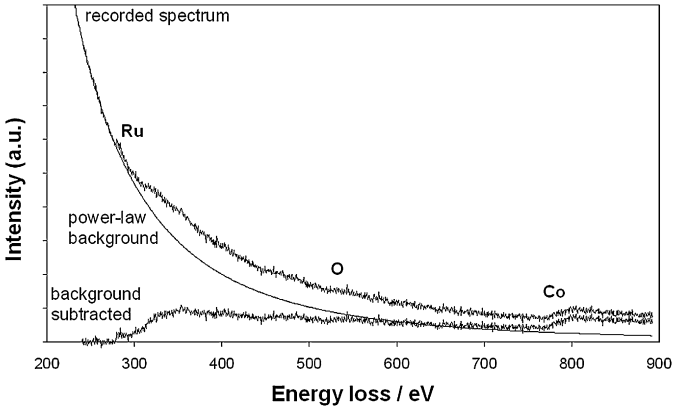

Fig. 6. Sum of 30 EELS spectra at the centre of Co particle, the fitted power law background and the background subtracted result.

the number of atoms is observed and can be used to deduce information on the shape of the particle of cobalt. Thus, the effect of the addition of the heavy atom is less than this simple proportionality to Z^2 would imply. In fact, taking into account the XRD evidence indicating that the Co metal particle is derived from a single Co_3O_4 crystallite, the visibility of PGM atoms should be similar in the reduced and calcined states, contrary to the experimental evidence.

The HAADF intensity was calculated for an idealized model of a Co particle (Fig. 9) using the multislice formalism embodied in the TEMSLIC software package [24]. The image simulations (Fig. 10) are based on elastic scattering from atoms in fixed positions and do not take into account thermal diffuse scattering directly. TEMSLIC can use a frozen phonon model to represent this by adding repeated calculations with small atom displacements from equilibrium, but no significant difference was found by incorporating this. The simulations are for random Re distribution on Co lattice sites in the whole particle (Fig. 10a) and in the surface layer (Fig. 10b). Note that the dopant atom positions are relatively weighted toward the edge in the (projection) image of the surface distribution compared with the bulk distribution.

Both HAADF simulations indicate that although the scattering by Co atoms is to first order proportional to the number of atoms in the atomic column, the visibility of the heavy atom depends on the position of this atom in the column with respect to the electron source. Promoter atoms at or near the entrance surface for the electron beam appear to contribute little more than a cobalt atom to the final signal and develop very little contrast, whereas those near the exit surface produce significant contrast. This holds for Re, Ir, and Pt, but for Ru the contrast is very low wherever the atoms are located [1].

This phenomenon was first reported only recently [10]. The variation with depth has been proposed as method for measuring the depth position of dopant atoms, although this assumes that reasonable Z contrast is present and is probably applicable only to samples of uniform thickness. Nevertheless, it is a surprising result. Electrons incident on a column of atoms are expected to be focused by those atoms and to channel along the column; however, the heavy atom must scatter so strongly that the focused beam that goes forward is diminished in strength, and so the scattered intensity arising from subsequent cobalt atoms along the column is weaker than if the heavy promoter atom had been another cobalt. The net effect is that the heavy

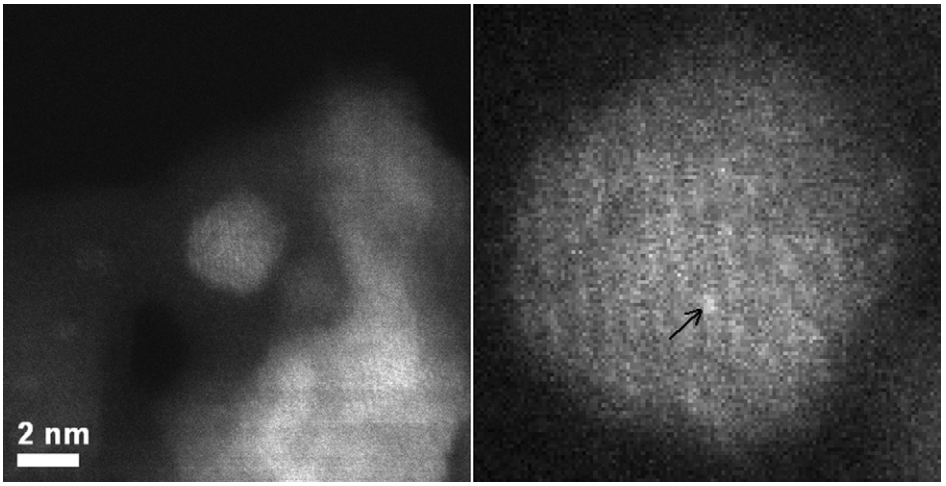

Fig. 7. HAADF image of a cobalt metal particle (centre left) and enlarged on the right showing a single bright atom sized feature (arrowed).

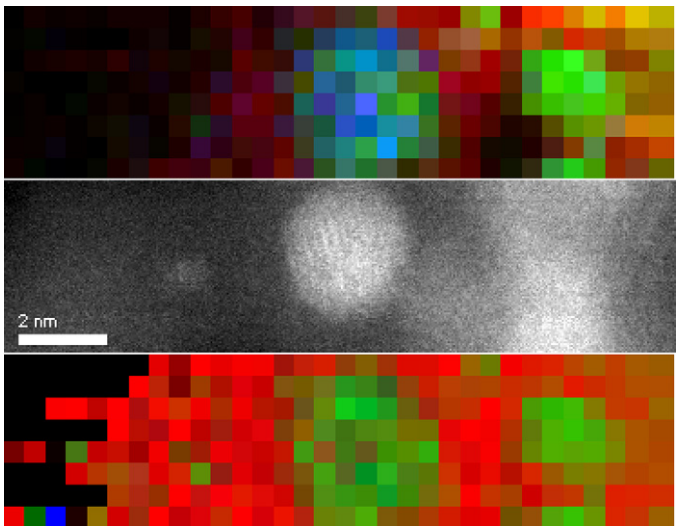

(a)

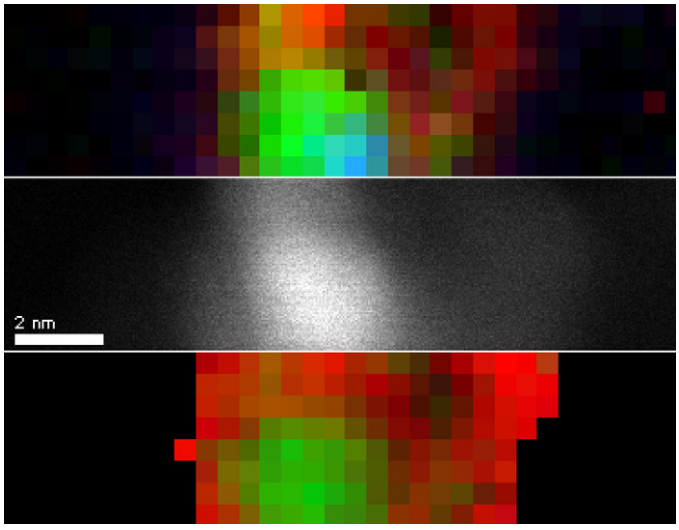

(b)

Fig. 8. Examples of Ru distribution determined by EELS spectrum imaging. In each group the HAADF image is in the centre and the colour images above and below are colour coded as O—red, Co—green and Ru—blue. (O is from the oxide support.) In the upper images the elements are scaled to give full colour where the maximum signal from that element occurs whereas in the lower images the intensity of the colour represents the local atom percent abundance. In (a) Ru is about 3% of the Co in the particle at the centre but absent from the particle to the right; in (b) Ru is associated with only part of the cobalt particle. (For interpretation of the references to colour in this figure legend, the reader is referred to the web version of this article.)

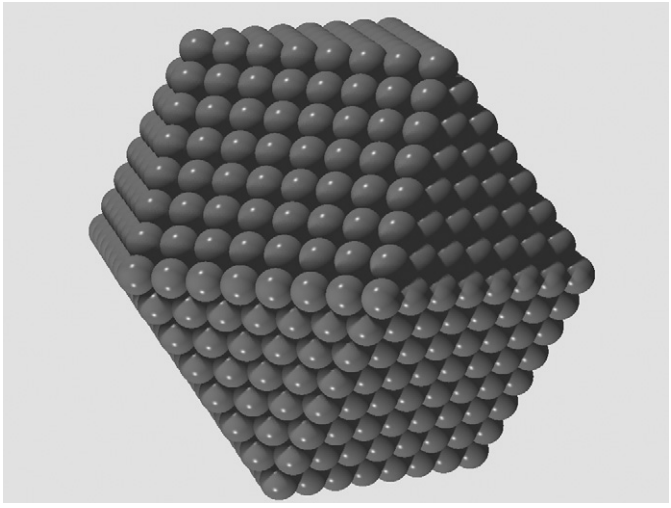

(a)

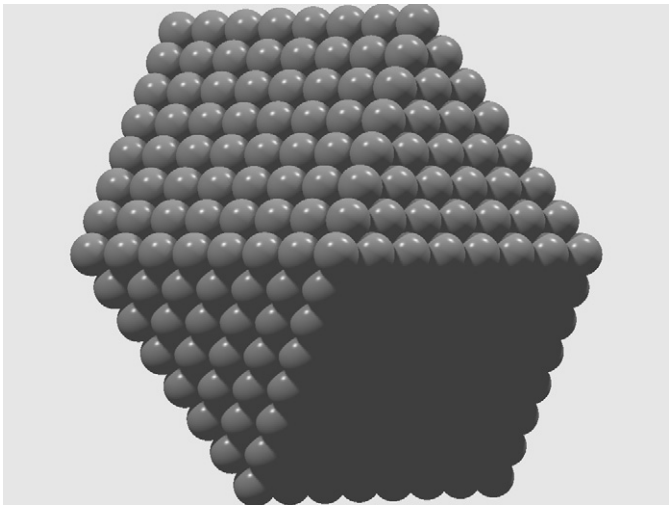

(b)

Fig. 9. (a) Idealised model of a Co particle with {111} and {200} facets and (b) its orientation in the simulations of Fig. 10.

atom is not readily detected when at or near the beam entrance face of a particle.

Other factors can influence the visibility of the promoter atoms. The nature of the samples makes it very difficult to find particles of cobalt protruding from the edge of a small agglomerate such that there is no alumina support under or above the cobalt particle being imaged, which acts to reduce the contrast of the promoter atom. Hydrocarbon contamination of the particle surface is known to affect the coupling of the focused probe into the atomic columns. The passivation layer on these samples may act in the same way and reduce the contrast.

Detecting interstitial promoter atoms requires good-quality BF and HAADF images along zone axes. This was rarely achieved with our samples. Some authors [25] have suggested that lattice images in aberration-corrected STEM are obtained over very large misorientations from the zone axis, citing polycrystalline silicon as an example in which almost all grains present a lattice image. However, in the samples studied here, not all cobalt crystals display even a lattice image, let alone an approximate zone axis. This may imply that the passivation layer destroys the electron channelling in most particles.

Passivation creates a monolayer or so of oxide coating. Any PGM atoms in the surface will become part of this. Presumably this layer is disordered, and the PGM atoms are rarely in lattice sites relative to the Co metal particle. They also may be extremely mobile. Consequently, the electron probe is not well coupled into the atom columns and planes and fewer particles than expected display these, thus hindering imaging of the heavy atoms. If so, then further progress in understanding the role of PGM promoters in FT catalysis will require reduction

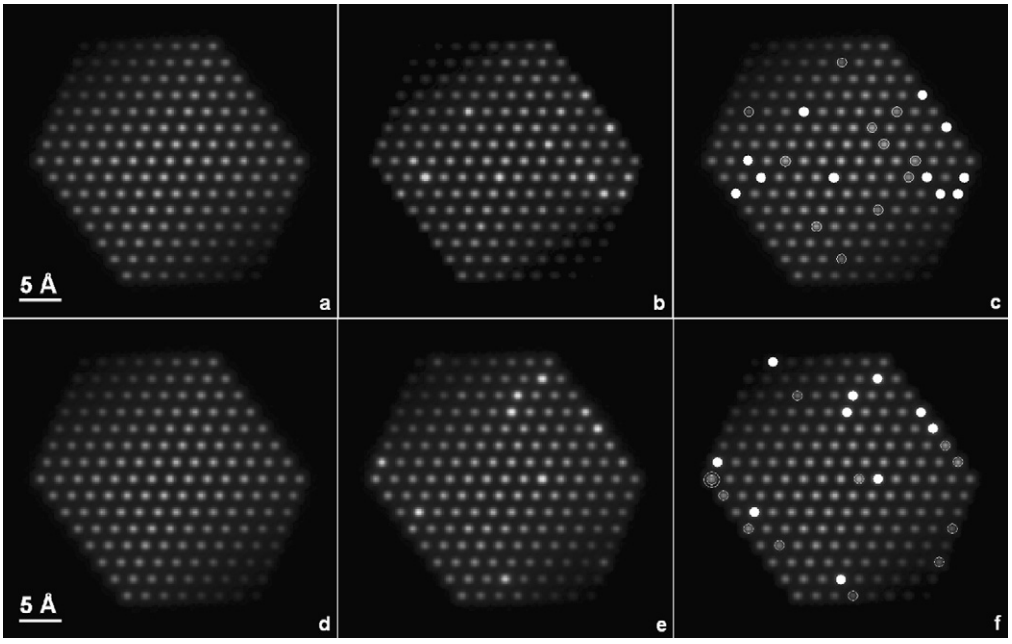

Fig. 10. Simulations of the HAADF image of an idealised 3 nm Co particle. (a) and (d) are of the undoped particle, (b) and (e) are randomly doped with Re in the bulk and in the surface layer respectively (see text), and (c) and (f) indicate the positions of the dopant atoms in projection with the solid circle representing a dopant atom in the upper half of the particle (near the exit surface in the imaging process) and the open circle representing those in the lower half of the particle (near the entrance surface in the imaging process).

or re-reduction of the passivated samples either in an ex situ gas reaction cell with vacuum transfer or by in situ reduction. A byproduct of the new technology of aberration correction is that more space for such devices can be made available.

Even if this is implemented, for electron optical reasons, not all heavy promoter atoms will be detected by HAADF aberration-corrected STEM imaging. There is a bias toward atoms located at or near the exit surface and those in lattice positions. This bias necessitates the development of other methods for detecting and identifying dopant atoms.

4.2. EELS spectrum imaging/EDX

The low-loss 0–120 eV region is useful for mapping out cobalt (Co-$M_{4,5}$ edge at 60 eV) and alumina (Al-$L_{2,3}$ edge at 75 eV). It is rapid, and pixel dwell times of 10 ms or less may be sufficient for mapping these two elements. All of the PGM metal promoters discussed here except Ru have an edge at 40–60 eV. Of course, at these low energies, there is some spatial delocalization of the signal to a few Angstroms; nonetheless, it was felt that useful information on promoter atom location still might be gleaned. But there was too much variability in this energy window and also at lower energy, due to collective excitation of electrons (plasmons), to be confident of single-atom detection. Although detection of larger clusters of atoms, as occur for Ru, might have been expected, significantly, none were found.

For the case of Ru promotion, Ru-$M_{4,5}$ (279 eV), O-K (530 eV), and Co-$L_{2,3}$ (779 eV) edges can be collected simultaneously with a dispersion of 0.5 eV. Moreover, cross-sections are available for these edges that permit quantification of the EEL spectra. O is a marker for the alumina support when the Co is present as the metal. Approximate quantification of the Ru and Co edges for the "patches" associated with Co particles and the reasonable assumption that the Co particles are spherical suggest that the Ru is present in islands on Co particles at a thickness of one monolayer or at most two monolayers.

Simulation shows that a single Ru dopant atom would be very difficult to detect by HAADF imaging unless present near the exit surface of the crystal. Therefore, single-atom detection by EELS is the key to further progress.

4.3. Relevance for catalysis

TPR had already demonstrated that the current method of depositing promoters by postdosing to the oxidic catalyst is effective in significantly lowering the reduction temperature of all cobalt species present, at least for the promoter levels currently applied (Table 1; Fig. 2). This is despite the fact that in this study, promoter-free cobalt particles were observed in the ruthenium-promoted catalyst. This observation is in line with the findings of Davis and co-workers [8,9] that no direct contact between the promoter and the cobalt particle is required, suggesting a mechanism of hydrogen spillover. Making a definitive statement on this requires confirmation that some cobalt particles are indeed promoter-free and quantification of their number, however.

The preparation method was also effective in increasing the Co surface area by at least 10 and 25% in the case of Ir. Therefore, the catalysts would be expected to show enhanced activity in FT synthesis [6]. The samples studied here were produced for microscopy experiments, however, and detailed catalytic performance data on them are not available.

5. Conclusion

Aberration-corrected STEM using the HAADF signal is capable of imaging some of the heavier PGM promoter atoms (i.e., Re, Ir, and Pt). Although positive identification of the atom type by EELS using low-energy edges was not successful, this information is not essential to progress in catalysis studies. What is essential, however, is to understand why not all of these PGM atoms can be imaged and to be able to compensate for this deficiency in interpretation. It is likely that the passivation layer on the samples studied here has rendered atoms invisible that otherwise might have been visible.

On the other hand, Ru was identified by EELS spectrum imaging in patches on Co particles. In this case, the intrinsic contrast in HAADF is unlikely to be large enough for studies based solely on this signal.

No isolated PGM atoms were found on the alumina support after reduction. In the Ru-promoted sample studied, the loading was in considerable excess of the optimum. In this case, although very small particles with very high Ru content were found on the alumina support, careful examination showed that none were Co-free.

Significant progress in this study is likely to require imaging of fully reduced samples. The ideal would be in-situ reduction from the oxide precursor, but ex situ reduction and vacuum transfer would be a useful interim step. Commercially viable catalysts prepared following the patent literature can be studied, as here, and are more representative than model systems.

Acknowledgments

The U.K. SuperSTEM facility (instrumentation and staff) is funded by the U.K. Engineering and Physical Sciences Research Council (EPSRC); additional funding was provided by Johnson Matthey (JM). The authors thank Andrew Bleloch, Technical Director of the facility, for useful discussions; Jill Turner and Sharon Bale for preparation of the catalysts, and Rob Fletcher and Sandra Riley (all of JM) for reduction and passivation of these; Steve Norval (ICI Measurement Science Group) for the in situ XRD data; and Patricia Kooyman (Delft) for the HRTEM particle sizing.

References

[1] J. Wall, J. Langmore, M. Isaacson, A.V. Crewe, Proc. Natl. Acad. Sci. USA 71 (1974) 1.
[2] P.E. Batson, N. Delby, O.L. Krivanek, Nature 418 (2002) 617.
[3] R. Oukaci, A.H. Singleton, J.G. Goodwin, Appl. Catal. A 186 (1999) 129.
[4] Syngas Refiner, Zeus Development Corporation ii (4) (2006).
[5] E. Iglesia, Appl. Catal. A 161 (1997) 59.
[6] C.M. Lok, Stud. Surf. Sci. Catal. 147 (2004) 283.
[7] G.L. Bezemer, J.H. Bitter, H.P.C.E. Kuipers, H. Oosterbeek, J.E. Holewijn, X. Xu, F. Kapteijn, A.J. van Dillen, K.P. de Jong, J. Am. Chem. Sci. 128 (12) (2006) 3956.
[8] G. Jacobs, J.A. Chaney, P.M. Patterson, T.K. Das, B.H. Davis, Appl. Catal. A 264 (2004) 203.
[9] G. Jacobs, J.A. Chaney, P.M. Patterson, T.K. Das, J.C. Maillot, B.H. Davis, J. Synch. Rad. 11 (2004) 414.
[10] P.M. Voyles, J.L. Grazul, D.A. Muller, Ultramicroscopy 96 (2003) 251.
[11] S. Wang, A.Y. Borisevich, S.N. Rashkeev, M.V. Glazoff, K. Sohlberg, S.J. Pennycook, S.T. Pantelides, Nature Mater. 3 (2004) 143.
[12] M. Varela, S.D. Findlay, A.R. Lupini, H.M. Christen, A.V. Borisevich, N. Delby, O.L. Krivanek, P.D. Nellist, M.P. Oxley, L.J. Allen, S.J. Pennycook, Phys. Rev. Lett. 92 (2004) 095502.
[13] C.M. Lok, M.D. Shannon, J.L. Casci, Europacat-VII, Book of Abstracts, Paper O2-17, Sofia (2005).
[14] G.L. Bezemer, U. Falke, A.J. van Dillen, K.P. de Jong, Chem. Commun. (2005) 731.
[15] G.L. Bezemer, P.B. Radstake, V. Koot, A.J. van Dillen, J.W. Geus, K.P. de Jong, J. Catal. 237 (2006) 291.
[16] P. Li, J. Liu, N. Nag, P.A. Crozier, Microsc. Microanal. 10 (2004) 470.
[17] P. Li, J. Liu, N. Nag, P.A. Crozier, Appl. Catal. A General 307 (2006) 212.
[18] R.L. Bonne, C.M. Lok, US Patent 5,874,381 (1999).
[19] C.M. Lok, G. Gray, G.J. Kelly, US Patent 6,927,190 (2005).
[20] Operators Manual for the Micromeretics ASAP 2010 Chemi System V 2.01, Appendix C, Part No. 201-42808-01, October 1996.
[21] O.L. Krivanek, N. Delby, A.R. Lupini, Ultramicroscopy 78 (1999) 1.
[22] C.M. Lok, S.V. Norval, Abstracts of 18th North American Catalysis Symposium at Cancun, National Science Foundation (2003) 294.
[23] Z.L. Wang, J. Bentley, N.D. Evans, Micron 31 (2000) 355.
[24] E.J. Kirkland, Advanced Computing in Electron Microscopy, Plenum Press, New York, 1998.
[25] P. Wang, A.L. Bleloch, U. Falke, P.J. Goodhew, Ultramicroscopy 106 (2006) 277.